Front. Optoelectron. China 2009, 2(2): 141–145
DOI 10.1007/s12200-009-0012-1

RESEARCH ARTICLE

Differential absorption optical coherence tomography with strong absorption contrast agents of gold nanorods

Ming WEI, Jun QIAN, Qiuqiang ZHAN, Fuhong CAI, Arash GHARIBI, Sailing HE (✉)

Centre for Optical and Electromagnetic Research, Joint Research Center of Photonics of the Royal Institute of Technology (Sweden) and Zhejiang University, Zhejiang University, Hangzhou 310058, China

Abstract Plasmon-resonant gold nanorods (GNRs) are demonstrated as strong absorption contrast agents for optical coherence tomography (OCT). OCT imaging of tissue phantoms doped with GNRs of different resonant wavelengths and concentrations is studied. To utilize the high absorption property of GNRs, a differential absorption OCT imaging is introduced to retrieve the absorption information of GNRs from conventional backscattered signals. It is shown that the contrast of the OCT image can be enhanced significantly when the plasmon resonant wavelength of the GNRs matches the central wavelength of the OCT source.

Keywords optical coherence tomography (OCT), plasmon resonance, gold nanorod (GNR), differential absorption

1 Introduction

Optical coherence tomography (OCT) is a non-invasive biomedical imaging technique that provides real-time (superior to such as computed tomography) and depth-resolved (superior to such as photoacoustic tomography) structural images with reasonable penetration depth (about 2 mm) and high spatial resolution (about 10 μm) [1]. Highly scattering microbubbles [2] and microspheres [3] have been developed as contrast agents to enhance the OCT signals for potential applications in such as specific targeting of molecular markers [4].

Gold nanoparticles are especially appealing as OCT contrast agents because they are less toxic [5], easier to synthesize, and more cost-effective [6] compared with other molecular markers such as fluorescent molecules and quantum dots. Besides many other advantages, nanoparticles with small sizes (typically < 100 nm) like gold nanorods (GNRs) with sharp spectral linewidths [7] (the spectral response of gold nanoshells [8] is too broad, full width at half maximum (FWHM) > 200 nm) and small sizes (much smaller than some other nanoparticles, such as nanoshells [8] or nanocages [9], etc.) are more desirable for spectroscopic OCT (SOCT) [10] as biomedical contrast agents. The longitudinal plasmon resonances of GNRs can be conveniently tuned (by adjusting their aspect ratio of length to diameter) to cover a large range from 525 to more than 1400 nm [11,12], which are excellent working wavelengths for OCT sources. Recently, GNRs have been developed as contrast agents for OCT [13], and gold nanoparticles are detected by photothermal methods [14,15]. As contrast agents, however, most of these GNRs are of highly scattering type, and they are difficult to synthesize near infrared spectrum and must be used with a large dosage (to get a high enough contrast) in highly scattering medium like tissues. For smaller-size GNRs, absorption contributes much more to the extinction loss than scattering. For instance, the scattering magnitude is less than 10% of the absorption for GNRs with effective radius $r_{\text{eff}} = 11.43$ nm and various aspect ratios (length-to-diameter) [16]. These high-absorption GNRs are about five times smaller (in volume) than highly scattering GNRs [13] and more than 10 times smaller than gold nanoshells [8]. Thus, they are easier to penetrate into tissues and greater dosages can be allowed (if needed) [17] for *in vivo* applications. These GNRs also have the potential for photothermal therapy [18] due to their strong absorption. Primarily, the depth-dependent OCT signal is dictated by the tissue with optical backscattering and extinction coefficients. However, when these high-absorption GNRs are used to target molecular markers of interest, like some specific tumors, it is difficult to clearly discriminate them from the targeted part. To take advantage of the high absorption of GNRs, a fundamental question is how to retrieve the strong absorption information of GNRs. In this

Received October 16, 2008; accepted December 3, 2008

E-mail: sailing@kth.se

article, we use small-sized GNRs (effective radius < 13 nm) as strong absorption contrast agents (instead of scattering contrast agents) to greatly enhance the contrast of OCT images. Furthermore, we introduce a mechanism called differential absorption OCT imaging, to retrieve the absorption information from conventional OCT signals.

2 Experiment and discussion

Cylindrical GNRs of various aspect ratios were synthesized in a manner similar to that reported by El-Sayed et al. [19]. Transmission electron microscope (TEM) images were taken by a JEOL JEM-1200EX transmission electron microscope for as-synthesized GNRs with a longitudinal resonant peak at 945 nm [Fig. 1(a)] and 666 nm [Fig. 1(b)]. Absorption spectra of the obtained nanorods were measured using ocean Optics S2000 miniature fiber optic spectrometer and are shown in Fig. 1(c).

A time-domain OCT system (shown in Fig. 2) was used in our experiment. A super-luminescence diode (SLD) centered at 1030 nm (with a bandwidth of about 80 nm) was used as the light source and its maximum output power was 5 mW. The axial in-focus and transverse resolutions were 8 and 12 μm, respectively.

To demonstrate the potential of GNRs as contrast agents, we performed OCT imaging on a tissue phantom of gelatin/TiO_2/India ink [20]. Unlike intralipid suspensions, a gelatin-based phantom allows for independent adjustment of optical properties by adjusting the ratio of TiO_2 and India ink amounts. Gelatin phantom with a back-scattering coefficient μ_s of 12.5 cm^{-1} and an absorption coefficient μ_a of 0.6 cm^{-1} was prepared by mixing 50 g gelatin powder, 450 mL water, 0.4 g TiO_2, and 0.2 mL India ink together.

Cross-sectional images of the tissue phantom doped with different concentrations of GNRs were obtained, and the influence of GNRs on the OCT imaging is shown in

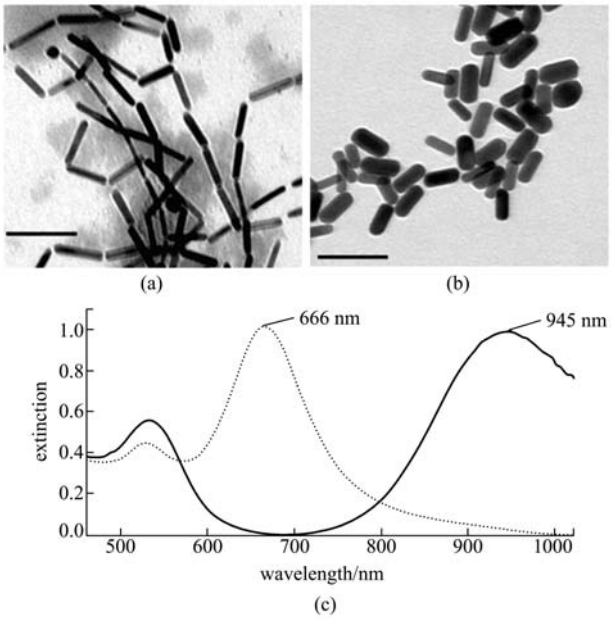

Fig. 1 TEM pictures of GNRs with longitudinal resonant peak at (a) 945 nm and (b) 666 nm (scale bars are 100 nm), and (c) extinction spectra of these two GNRs samples [solid line: GNRs shown in (a); dashed line: GNRs shown in (b)]

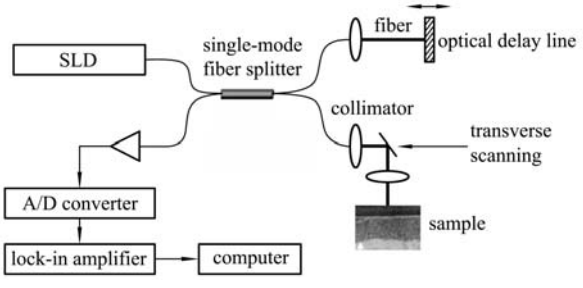

Fig. 2 Setup of time-domain OCT system

Fig. 3(a). Herein the longitudinal resonant peak of GNRs is at 945 nm, which matches well with the central wavelength of the OCT light source. The concentrations of GNRs in the phantom were 8 pmol/mL (Part 1), 5 pmol/mL (Part 2), and 0 pmol/mL (Part 3), respectively. We use the following expression for the total extinction coefficient $\mu_{\text{ext,total}}$ of the medium (assuming the independent scattering approximation [21] holds):

$$\mu_{\text{ext,total}} = (\mu_{\text{s,TiO}_2} + \mu_{\text{a,TiO}_2})f_{\text{TiO}_2} + (\mu_{\text{s,GNRs}} + \mu_{\text{a,GNRs}})f_{\text{GNRs}}, \quad (1)$$

where $\mu_{\text{s,TiO}_2}$ and $\mu_{\text{a,TiO}_2}$ are the backscattering and absorption coefficients of the phantom with TiO_2 only, and $\mu_{\text{s,GNRs}}$ and $\mu_{\text{a,GNRs}}$ are the backscattering and absorption coefficients of the GNRs, respectively; f_{TiO_2} and f_{GNRs} are the fractional volumes of TiO_2 and GNRs, respectively.

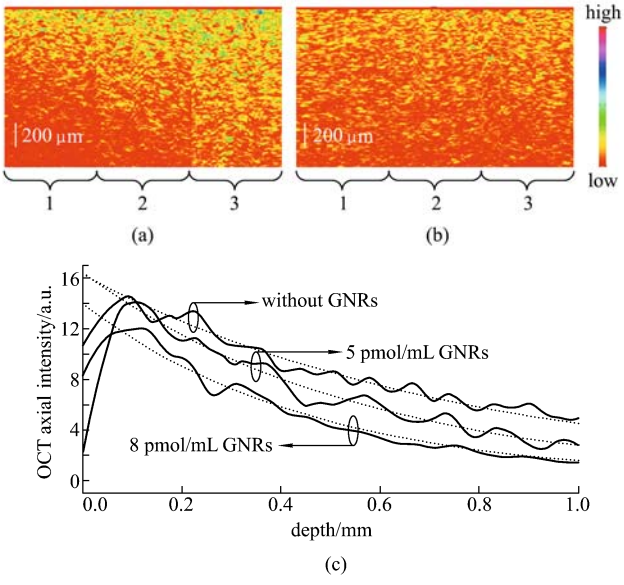

Fig. 3 (a) Cross-sectional OCT images of tissue phantom doped with GNRs with resonance at 945 nm. Concentrations of GNRs in different parts of phantom (from left to right) are: 8 pmol/mL (Part 1), 5 pmol/mL (Part 2), and 0 (Part 3); (b) cross-sectional OCT images of tissue phantom doped with GNRs with resonance at 666 nm. Concentrations of GNRs are the same as those in (a), vertical scale bars are 200 μm; (c) demodulated OCT intensities decay with their best-fit lines (dashed lines) for different concentrations of GNRs used in (a)

The demodulated OCT signal S_{OCT} is proportional to the electric field magnitude scattered from the medium at a depth of z below the surface of the phantom. It can be written as [22]

$$S_{\text{OCT}}(z) = S_0\sqrt{\mu_{\text{bs}}(z)}\exp[-\mu_{\text{ext,total}}(z)z]h(z),$$
$$h(z) = 1/[1 + (z - z_{\text{f}})^2/(\alpha z_0)^2]^{1/2}, \quad (2)$$

where S_0 is a system parameter determined by the sensitivity of the OCT system; $\mu_{\text{bs}}(z)$ is the 180 degree backscattering coefficient [23], $h(z)$ is the point spread function describing the focusing effect of a Gaussian beam (z_{f} represents the focus position, z_0 is the Rayleigh range, and α accounts for the influence of scattering in the Rayleigh range). A typical backscattered intensity profile and the corresponding fitting curve are shown in Fig. 3(c) according to Eq. (2). The fitted $\mu_{\text{ext,total}}$ are 1.285 mm^{-1} (Part 3), 1.782 mm^{-1} (Part 2), and 2.196 mm^{-1} (Part 1), respectively. It is clear that the demodulated OCT signals decay faster (i.e., $\mu_{\text{ext,total}}$ become larger) when the concentrations of GNRs increase, owing to the strong absorption by GNRs according to Eq. (1). In Fig. 3(b), however, unlike Fig. 3(a), the penetration depth does not change much for different concentrations of GNRs with resonance at 666 nm. This is because the resonant wavelength of the GNRs used in Fig. 3(b) is outside the spectral envelope of the OCT source, and consequently the absorption effect is not obvious.

Next we used a two-layered tissue phantom as a sample. Figure 4(a) shows conventional OCT signals of the backscattering intensity inside the measured phantom. The two layers are separated by a red solid line. The part inside the square corresponds to the part of the phantom doped with 2 pmol/mL concentration of GNRs resonant at 945 nm, and the rest part corresponds to the phantom part without GNRs. It can be seen that the penetration depth of the left part is less than that of the right part. However, if the layer inside the square is very thin, we can hardly see any difference between phantoms with and without GNRs, because the measurement of backscattering alone does not permit the discrimination of high-absorption GNRs.

To improve the contrast of the OCT image by taking advantage of the strong absorption property of GNRs, we introduce a contrast mechanism, differential absorption OCT imaging. First, we gave a reference phantom which contains the same material (but thicker) as the upper layer of the measured phantom and then measured its fitted extinction coefficient $\mu'_{\text{ext0,ref}}$ according to Eq. (2), and its result is shown in Fig. 4(c). It then follows that the absorption signal of each layer can be described as [cf. Eq. (2)]

$$\begin{aligned}\Delta\mu_{\text{ext,total}}(z) &= \mu_{\text{ext,phantom}}(z) - \mu_{\text{ext,ref}}(z)\\ &= -\frac{1}{z - z_l}\log\frac{S_{\text{OCT}}(z)h(z_l)}{S_{\text{OCT}}(z_l)h(z)}\\ &\quad - \left[-\frac{1}{z - z_l}\log\frac{S_{\text{OCT,ref}}(z)h(z_l)}{S_{\text{OCT,ref}}(z_l)h(z)}\right]\\ &= -\frac{1}{z - z_l}\log\frac{S_{\text{OCT}}(z)}{S_{\text{OCT}}(z_l)} - \mu'_{\text{ext0,ref}},\end{aligned}$$

where $\Delta\mu_{\text{ext,total}}(z)$ is the differential extinction coefficient between the measured phantom [same as Fig. 4(a)] and the reference phantom; $\mu_{\text{ext,phantom}}(z)$ and $\mu_{\text{ext,ref}}(z)$ are the extinction coefficients of the measured phantom and the

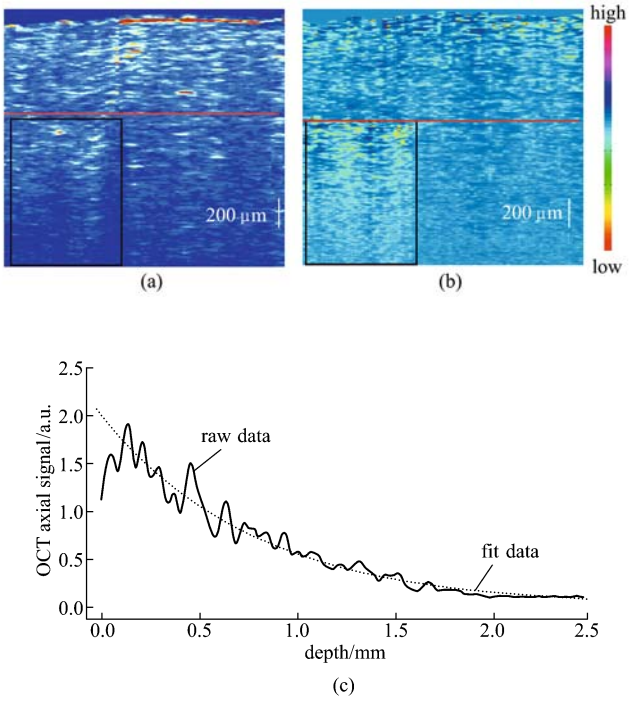

Fig. 4 Conventional OCT signals of two-layer phantom indicative of (a) backscattered intensity (the two layers are separated in a red solid line) and (b) differential absorption signal (the layer inside the square of the image is phantom doped with GNRs resonant at 945 nm at a concentration of 2 pmol/mL, scale bars are 200 μm); (c) demodulated OCT intensity decay with their best-fit lines (dashed lines) of phantom with TiO_2 only

reference phantom, respectively; $S_{OCT}(z)$ and $S_{OCT,ref}(z)$ are the demodulated OCT signals of the measured phantom and the reference phantom, respectively; and z_l is the depth at the upper surface of the lth layer.

To eliminate the contribution from TiO_2, we fix f_{TiO_2} in Eq. (1) the same value for all phantoms. Furthermore, as the backscattering cross section of GNRs is several orders of magnitude smaller than the absorption cross section, we can ignore the contribution of scattering to the extinction loss of GNRs. It then follows from Eq. (1) that $\Delta\mu_{ext,total} = \mu_{ext,phantom} - \mu_{ext,ref} \approx \mu_{a,GNRs} f_{GNRs} = \Delta\mu_{a,GNRs}$, where the differential absorption magnitude $\Delta\mu_{a,GNRs}(z)$ of GNRs is proportional to the concentration (f_{GNRs}) of GNRs in phantom. As a result, we obtain the differential absorption information $\Delta\mu_{a,GNRs}(z)$ [Fig. 4(b)] from the scattering image. Compared with Fig. 4(a), we can easily discriminate in Fig. 4(b) the part doped with GNRs from the rest phantom. Considering the layer with GNRs as some sort of pathological tissue whose scattering is almost the same as the surrounding tissue but with much higher absorption, we can still easily discriminate the part (even if this layer is very thin) from the rest [Fig. 4(b)], much better than the conventional OCT scattering image [Fig. 4(a)].

3 Conclusion

In summary, we experimentally demonstrated GNRs as strong absorption contrast agents in an OCT system. The major features of the GNRs attractive for OCT imaging are their less toxicity, strong absorption, the large tunable range of their longitudinal plasmon resonances, and sharp optical resonance spectrum compared with other molecular markers. We obtained significant enhancement of contrast with GNRs resonant at a wavelength within the spectral bandwidth of the OCT source. GNRs resonant at a wavelength outside the spectral envelope contribute little to the OCT signal. This result may be useful in multi-spectral OCT of molecular imaging using spectrally differential methods [24], where contributions of GNRs resonant at various wavelengths can be resolved and GNRs can be targeted to various markers of interest. Furthermore, we have shown that large absorption GNRs can be used in OCT system as absorption contrast agents. We identified a new contrast mechanism (differential-absorption OCT imaging) for OCT imaging based on the strong absorption of GNRs. It can retrieve the absorption information from conventional scattering information of OCT. By this mechanism, we obtain both absorption and scattering information, which can explore better the potential of OCT imaging for some pathological tissues. It is especially useful to discriminate objects doped with GNRs which give pretty small scattering but high absorption. For instance, if we target GNRs to some pathological tissues whose scatterings are almost the same as the surrounding tissues, we can use the present differential absorption method to detect the location and even shape of these tissues. For most tissues that are highly scattered but weakly absorptive medium, this mechanism can be used with small dosages of high-absorption GNRs as contrast agents.

Acknowledgements This work was partially supported by the National Natural Science Foundation of China (Grant No. 60688401) and partially supported by a multidisciplinary project of Zhejiang University and the Swedish Foundation for Strategic Research (SSF).

References

1. Huang D, Swanson E A, Lin C P, Schuman J S, Stinson W G, Chang W, Hee M R, Flotte T, Gregory K, Puliafito C A, Fujimoto J G. Optical coherence tomography. Science, 1991, 254(5035): 1178–1181
2. Barton J K, Hoying J B, Sullivan C J. Use of microbubbles as an optical coherence tomography contrast agent. Academic Radiology, 2002, 9(1): S52–S55
3. Lee T M, Oldenburg A L, Sitafalwalla S, Marks D L, Luo W, Toublan F J J, Suslick K S, Boppart S A. Engineered microsphere contrast agents for optical coherence tomography. Optics Letters, 2003, 28(17): 1546–1548

4. Boppart S A, Oldenburg A L, Xu C, Marks D L. Optical probes and techniques for molecular contrast enhancement in coherence imaging. Journal of Biomedical Optics, 2005, 10(4): 041208
5. Murphy C J, Gole A M, Stone J W, Sisco P N, Alkilany A M, Goldsmith E C, Baxter S C. Gold nanoparticles in biology: beyond toxicity to cellular imaging. Accounts of Chemical Research, 2008, 41(12): 1721–1730
6. Connor E E, Mwamuka J, Gole A, Murphy C J, Wyatt M D. Gold nanoparticles are taken up by human cells but do not cause acute cytotoxicity. Small, 2005, 1(3): 325–327
7. Sonnichsen C, Franzl T, Wilk T, Von Plessen G, Feldmann J, Wilson O, Mulvaney P. Drastic reduction of plasmon damping in gold nanorods. Physical Review Letters, 2002, 88(7): 077402
8. Zagaynova E V, Shirmanova M V, Kirillin M Y , Khlebtsov B N, Orlova A G, Balalaeva I V, Sirotkina M A, Bugrova M L, Agrba P D, Kamensky V A. Contrasting properties of gold nanoparticles for optical coherence tomography: phantom, *in vivo* studies and Monte Carlo simulation. Physics in Medicine and Biology, 2008, 53(18) 4995–5009
9. Cang H, Sun T, Li Z Y, Chen J, Wiley B J, Xia Y, Li X. Gold nanocages as contrast agents for spectroscopic optical coherence tomography. Optics Letters, 2005, 30(22): 3048–3050
10. Oldenburg A L, Hansen M N, Zweifel D A, Wei A, Boppart S A. Plasmon-resonant gold nanorods as low backscattering albedo contrast agents for optical coherence tomography. Optics Express, 2006, 14(15): 6724–6738
11. Jana N R, Gearheart L, Murphy C J. Wet chemical synthesis of high aspect ratio cylindrical gold nanorods. Journal of Physical Chemistry B, 2001, 105(19): 4065–4067
12. Huang X, El-Sayed I H, Qian W, El-Sayed M A. Cancer cell imaging and photothermal therapy in the near-infrared region by using gold nanorods. Journal of the American Chemical Society, 2006, 128(6): 2115–2120
13. Troutman T S, Barton J K, Romanowski M. Optical coherence tomography with plasmon resonant nanorods of gold. Optics Letters, 2007, 32(11): 1438–1440
14. Adler D C, Huang S, Huber R, Fujimoto J G. Photothermal detection of gold nanoparticles using phase-sensitive optical coherence tomography. Optics Express, 2008, 16(7): 4376–4393
15. Skala M C, Crow M J, Wax A, Izatt J A. Photothermal optical coherence tomography of epidermal growth factor receptor in live cells using immunotargeted gold nanospheres. Nano Letters, 2008, 8 (10): 3461–3467
16. Jain P K, Lee K S, El-Sayed I H, El-Sayed M A. Calculated absorption and scattering properties of gold nanoparticles of different size, shape, and composition: applications in biological imaging and biomedicine. Journal of Physical Chemistry B, 2006, 110(14): 7238–7248
17. Nel A, Xia T, Madler L, Li N. Toxic potential of materials at the nanolevel. Science, 2006, 311(5761): 622–627
18. Prescott S W, Mulvaneya P. Gold nanorod extinction spectra. Journal of Applied Physics, 2006, 99(12): 123504
19. Babak N, El-Sayed M A. Preparation and growth mechanism of gold nanorods (NRs) using seed-mediated growth method. Chemistry Materials, 2003, 15(10): 1957–1962
20. Swartling J, Dam J S, Andersson-Engels S. Comparison of spatially and temporally resolved diffuse-reflectance measurement systems for determination of biomedical optical properties. Applied Optics, 2003, 42(22): 4612–4621
21. Zaccanti G, Bianco S D, Marelli F. Measurements of optical properties of high-density media. Applied Optics, 2003, 42(19): 4023–4030
22. Van Leeuwen T G, Faber D J, Aalders M C. Measurement of the axial point spread function in scattering media using single-mode fiber-based optical coherence tomography. IEEE Journal of Selected Topics in Quantum Electronics, 2003, 9(2): 227–234
23. Schmitt J M, Knuttel A, Bonner R F. Measurement of optical properties of biological tissues by low coherence reflectometry. Applied Optics, 1993, 32(30): 6032–6042
24. Schmitt J M, Xiang S H, Yung K M. Differential absorption imaging with optical coherence tomography. Journal of the Optical Society of American A, 1998, 15(9): 2288–2296